

Precision cosmology with time delay lenses: high resolution imaging requirements

Xiao-Lei Meng,¹ Tommaso Treu,^{1,2} Adriano Agnello,^{1,2} Matthew W. Auger,³ Kai Liao,^{1,2} Philip J. Marshall⁴

¹Department of Physics, University of California, Santa Barbara, CA 93106, USA

²Physics and Astronomy Building, 430 Portola Plaza, Box 951547, Los Angeles, CA 90095-1547, USA

³Institute of Astronomy, UK

⁴Kavli Institute for Particle Astrophysics and Cosmology, Stanford University, 452 Lomita Mall, Stanford, CA 94305, USA

E-mail: xlmeng919@gmail.com

Abstract. Gravitational time delays are a powerful probe of cosmology, provided that the gravitational potential of the main deflector can be modeled with sufficient precision. Recent work has shown that this can be achieved by detailed modeling of the host galaxies of lensed quasars. The distortion of the images as measured over large number of pixels provides tight constraints on the difference between the gravitational potential between the two quasars, and thus on cosmology in combination with the measured time delay. We carry out a systematic exploration of the high resolution imaging required to exploit the thousands of lensed quasars that will be discovered by current and upcoming surveys with the next decade. Specifically we simulate realistic lens systems as imaged by the Hubble Space Telescope (HST), James Webb Space Telescope (JWST), ground based adaptive optics images taken with Keck or the Thirty Meter Telescope (TMT). We compare the performance of these pointed observations with that of images taken by the Euclid-VIS, Wide-Field Infrared Survey Telescope (WFIRST) and Large Synoptic Survey Telescope (LSST) surveys. Using as our metric the precision with which the slope of the mass density profile for the main deflector can be measured **we find that...**

Contents

1	Introduction	1
2	The Lens Sample	1
3	Instrument Simulations	2
4	Lens Reconstruction	2
5	Results	2
6	Summary	2

1 Introduction

[TT to put introfirst here, introduce ‘informative pixels’ that will be referred to in Sect.s 2 and 3]

This paper is organized as follows. We first introduce our lens sample in Section 2. Next, we briefly summarize a variety of telescopes properties used in this work and show simulated realistic lens systems as imaged by these telescopes in Section 3. The results from simulation in Section 4. Finally, we discuss and summarize our work in Section 5. Throughout this paper, all magnitudes are given in the AB system. Even though it is not crucial to our findings, we adopt a spatially flat Λ CDM cosmology with $\Omega_m = 0.3$, $\Omega_\Lambda = 0.7$, and the Hubble constant $H_0 = 70 \text{ km s}^{-1} \text{ Mpc}^{-1}$ when calculating distances.

2 The Lens Sample

We have chosen four prototypical systems for this exploration, characterized as *faint* or **bright** and **double** or **quad** depending on the photometry and image configuration. Their structural parameters are listed in Table 2. This set of four main choices covers regimes with different numbers of informative pixels, which depend on the S/N ratio and on the number of images produced by the lens.

To remain as realistic as possible, the mocks are based upon lenses in the SLACS (...) and SL2S (...) samples. When not explicitly known from existing data, mock model parameters are assigned via plausibility arguments as specified below. The source and deflector of the *bright* configurations are built along SLACS J0330-0020 as modelled by Auger et al.(SLACS11). For the *faint* configuration, the deflector has parameters from the Sonnenfeld et al. (????) model of SL2S J135949+553550. Source magnitudes in the *faint* case are arbitrarily set to 25.0 in all bands, whence the source effective radius R_{eff} is assigned along the size-magnitude relation given by Newton et al. (2011?). In all cases, the source positions are assigned so as to map the source in either two or four images. Unknown magnitudes in *K* band are assigned from *H*-band ones via $K_{AB} = H_{AB}$.

Question: What are the point-source magnitudes, even if they’re not specifically modelled? How were they assigned? Based on the recipe that Kai and I assembled? Also, magnitudes in the tables are not necessarily the instrument ones, how are they converted? With the XLM’s template-based table from AA?

Then: say that source is mapped onto lens plane with formalism illustrated later on, lens light is summed to it, noise added. Refer to one example of puppies, **including TMT with kernel smoothing**.

3 Instrument Simulations

Here we introduce the telescopes and instruments with their bands... Do some of them need special remarks? We should show a cutout of the PSF for each of them.

4 Lens Reconstruction

The deflector is assigned within a class of power-law density profiles,

$$\Sigma(x, y) = \dots \quad (4.1)$$

Here, illustrate the conventions used for deflection angles (refer to Barkana for fastell), hence define R_E . The mock deflector parameters are listed in Table 3... Lensed image profiles are obtained by Inverse Ray Shooting: each pixel position in the image plane is mapped back to the source plane via eq ... and surface-brightness conservation is exploited (**insert equations** $S B(\theta - \beta)$...).

The same code is used to generate the mock models and to fit them. The model fits the following parameters: **which ones?** Goodness of fit is assessed through the image-plane χ^2 , comparing the model and mock data surface brightness profiles. The quasar images are not used in the fit, which is made just on the lensed host. Uncertainties are obtained via MCMC exploration of the likelihood, which in this case is simply given by $\mathcal{L} \propto \exp[-\chi^2/2]$.

5 Results

6 Summary

Acknowledgments

References

- [1] A. S. Bolton, S. Burles, L. V. E. Koopmans, T. Treu, R. Gavazzi, L. A. Moustakas, R. Wayth, and D. J. Schlegel, *The Sloan Lens ACS Survey. V. The Full ACS Strong-Lens Sample*, *Astrophys. J.* **682** (Aug., 2008) 964–984, [[arXiv:0805.1931](https://arxiv.org/abs/0805.1931)].
- [2] M. W. Auger, T. Treu, A. S. Bolton, R. Gavazzi, L. V. E. Koopmans, P. J. Marshall, K. Bundy, and L. A. Moustakas, *The Sloan Lens ACS Survey. IX. Colors, Lensing, and Stellar Masses of Early-Type Galaxies*, *Astrophys. J.* **705** (Nov., 2009) 1099–1115, [[arXiv:0911.2471](https://arxiv.org/abs/0911.2471)].

Table 1. Telescope Properties

Telescope Name	Filter	Zero Point	Readout (-e/pixel/s)	Background (-e/pixel/s)	Pixel Scale (arcsec)
HST	F814W	25.94	4.20	0.11	0.050
JWST	F200W	27.85	9.00	0.20	0.032
Keck	NIRC2/K	28.04	5.75	25.94	0.010
NGAO	K	28.04	5.75	25.94	0.010
TMT	IRIS	31.10	2.00	21.20	0.004
Euclid	VIS	25.58	4.50	0.43	0.100
WFIRST	F184	26.18	5.00	0.11	0.110
LSST	I	28.35	5.00	68.00	0.200

Zero points used in this work are given in the ABmag system.

Table 2. Surface Brightness Profile Models

Lens Name	R_{eff} (arcsec)	q	P.A. (deg)	n	Δx (arcsec)	Δy (arcsec)	m_I	m_K	m_{VIS}	m_H
Parameters for the Source										
fainter system ^a	0.23	0.92	54.0	4.0	0.0662	-0.167	25.0	25.0	25.0	25.0
fainter system ^b	0.23	0.92	54.0	4.0	0.008	0.298	25.0	25.0	25.0	25.0
brighter system ^b	0.12	0.77	120.0	1.33	-0.195	0.34	22.73	22.0	23.46	22.0
brighter system ^a	0.12	0.77	120.0	1.33	0.01	-0.005	22.73	22.0	23.46	22.0
Parameters for the lens										
fainter system	1.76	0.61	-9.6	4.0	—	—	20.69	19.7	21.13	19.7
brighter system	0.91	0.81	113.2	4.0	—	—	17.99	16.5	18.84	16.5

The effective radius R_{eff} is the radius at which the major axis contains half of the total flux. q denotes the axis ratio. P.A. is with respect to the x-axis. The Sérsic index n controls the degree of curvature of the galaxy light profile. Magnitudes m are given in the ABmag system. The only difference among sources of different brightness is in the source-position, which is set to produce either two or four images.

^a 4 QSO images exist in the lens plane.

^b 2 QSO images exist in the lens plane.

Table 3. Lens Model Parameters

Lens Name	z	R_{Ein} (arcsec)	q	P.A. (deg)	γ'
fainter system	0.783	1.14	0.6	14.7	2.0
brighter system	0.351	1.1	0.81	113.2	2.0

Rephrase[R_{Ein} is the radius of a ring which is taken from a lensing phenomenon if a point source is located on the viewing direction extending from the observer]. q denotes the axis ratio. P.A. is anti-clockwise from the x-axis. The underlying deflector is a Singular Isothermal Ellipsoid ($\gamma'=2$), which will be fit using power-law models.

^a 4 QSO images exist in the lens plane.

^b 2 QSO images exist in the lens plane.

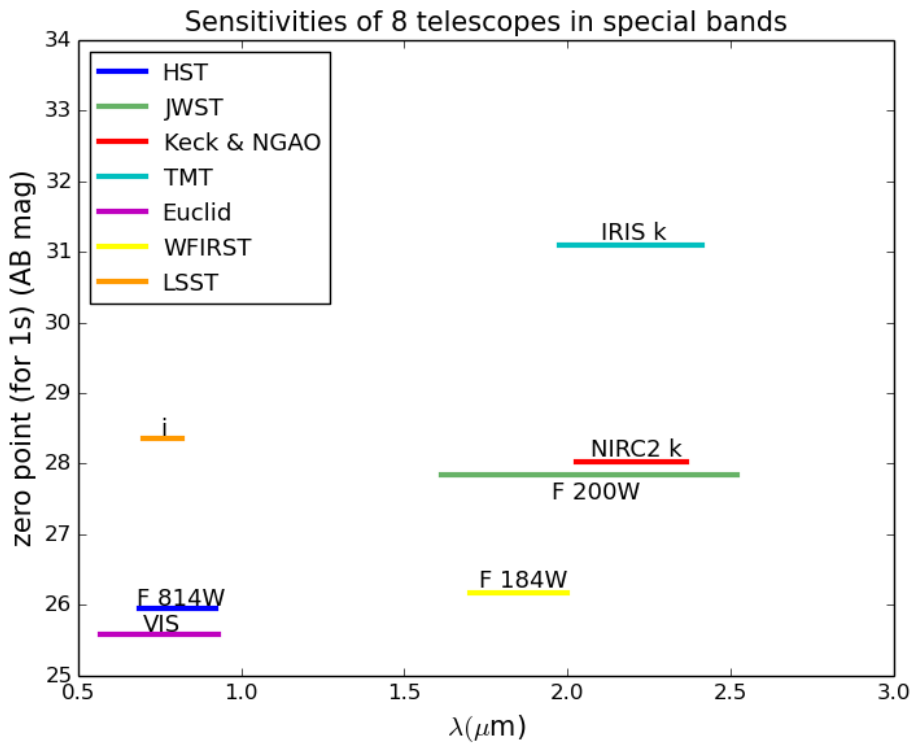


Figure 1. Zero Points in AB magnitudes of HST (blue), JWST (green), Keck & NGAO (red), TMT (cyan), Euclid (magenta), WFIRST (yellow) and LSST (orange) in units of per second. Different color bars indicate the wavelength range of each telescope used in this work.

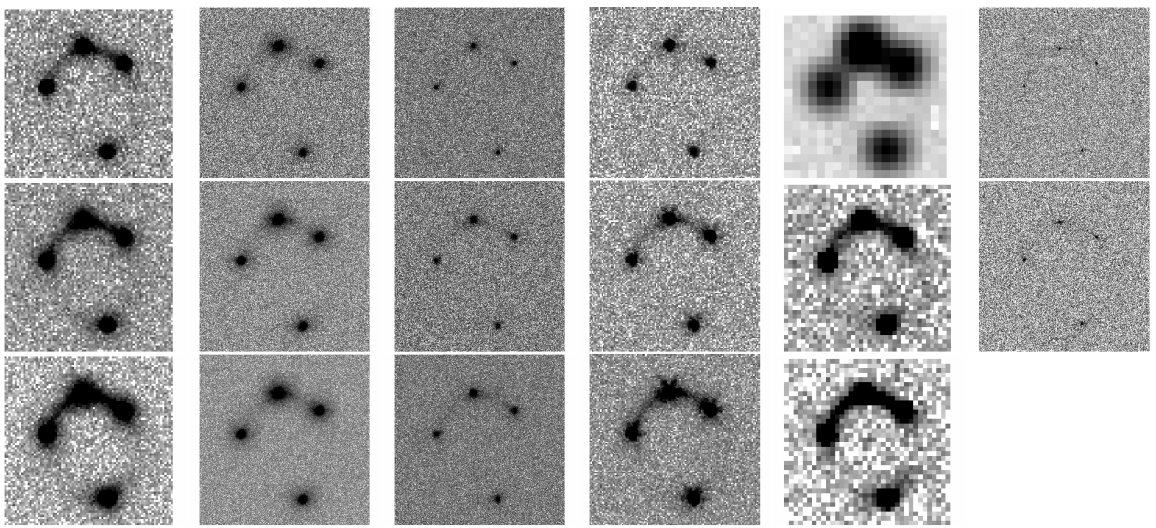


Figure 2. Simulated lens system results showing the fainter lens system (4 QSO images in the lens plane). The simulated image pixel scales are all $4'' \times 4''$. The first 4 columns, from left to right, represent HST, Keck, NGAO, and JWST; from top to bottom, correspond to $1/3 \times$ good exposure time, good exposure time, and $3 \times$ good exposure time (See the definition of “good exposure time” in Section *.*). The fifth column include 3 survey detections by 3 different telescopes, from top to bottom, for LSST, Euclid, and WFIRST respectively. The last column is for TMT with 2 fixed exposure time: 360 seconds and 1080 seconds.

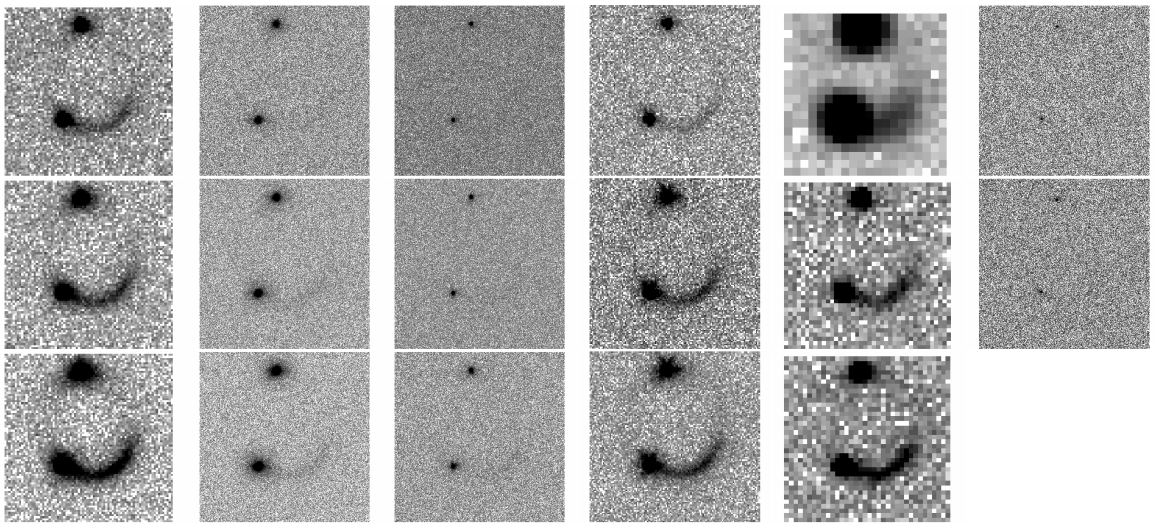


Figure 3. Same as Fig. 2, except that the simulated lens system results showing the fainter lens system (2 QSO images in the lens plane).

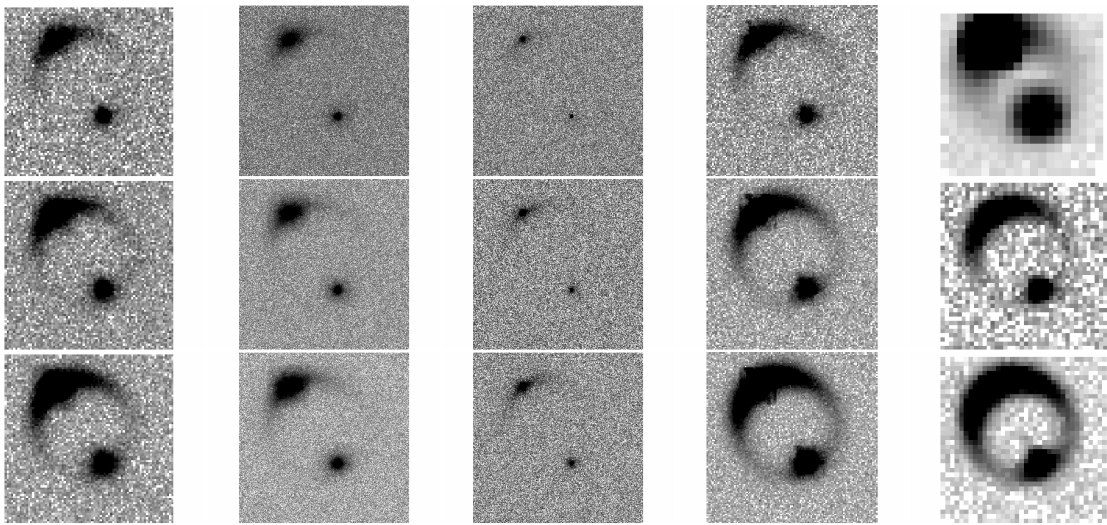


Figure 4. Simulated lens system results showing the brighter lens system (2 QSO images in the lens plane). The simulated image pixel scales are all $4'' \times 4''$. The first 3 columns, from left to right, present HST, Keck, and NGAO; from top to bottom, correspond to $1/3 \times$ good exposure time, good exposure time, and $3 \times$ good exposure time. The fourth column shows JWST with 3 fixed exposure time: 60 seconds, 180 seconds, and 540 seconds. The last column include 3 survey detections by 3 different telescopes, from top to bottom, for LSST, Euclid, and WFIRST respectively.

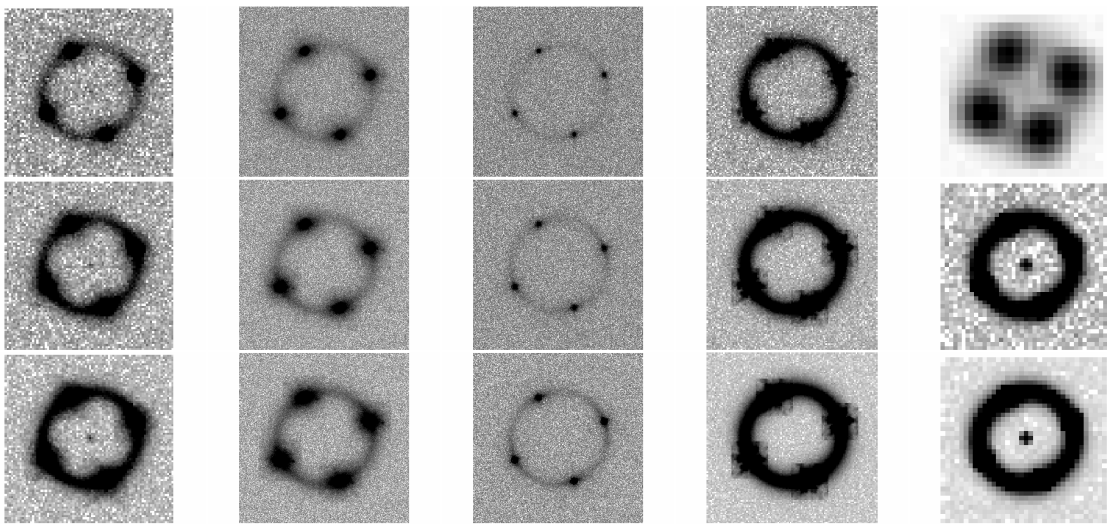


Figure 5. Same as Fig. 4, except that the simulated lens system results showing the brighter lens system (4 QSO images in the lens plane). The black spots in the center of the simulated images using HST, Euclid and WFIRST are from the efforts of strong signal pixels, so it's a “ghost” image which can be ignored.

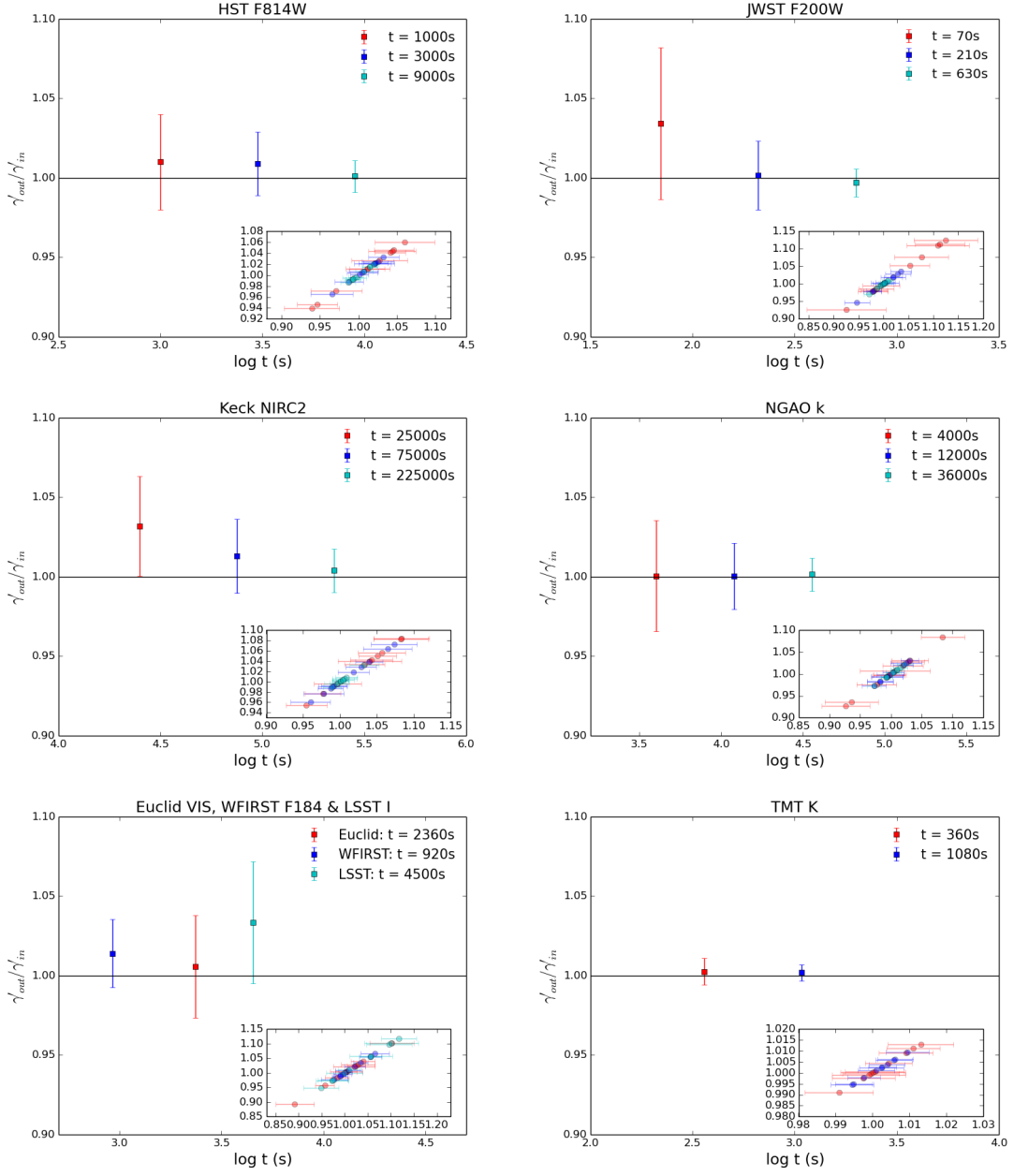


Figure 6. The ability of recovering mass slope with respect to different exposure time for a variety of telescopes. This figure shows the fainter lens system with 4 QSO images in the lens plane. γ'_{in} is the input SIE mass slope. γ'_{out} is drawn from MCMC sampling based on the simulated images given γ'_{in} . The error bar represents 1σ confidence range. The insert in each panel shows all 10 simulation results for each exposure time with the same color coding. Note that both axes represent $\gamma'_{out}/\gamma'_{in}$ whereas error bars are only shown on the x-axis for clarity.

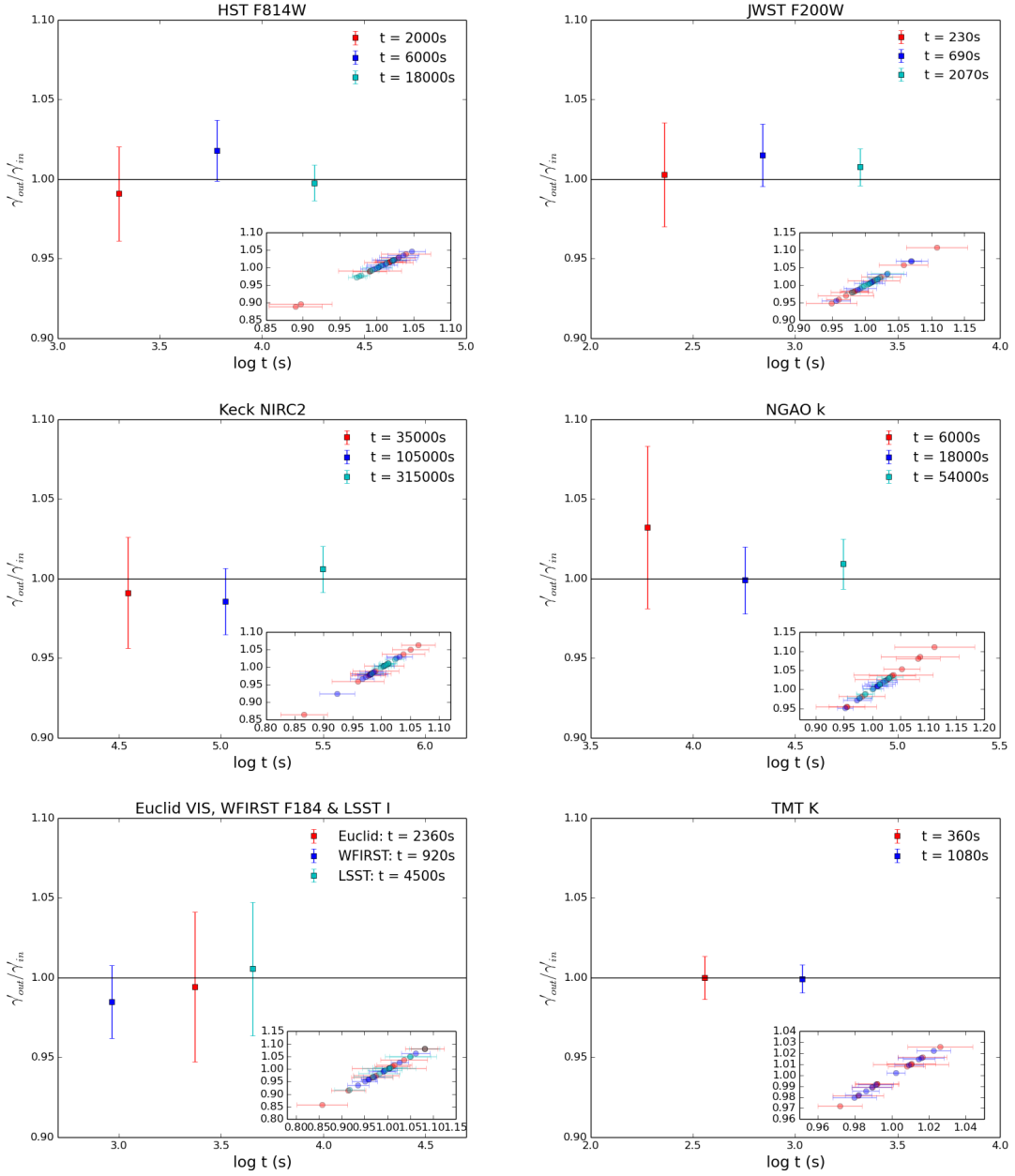


Figure 7. Same as Fig. 6, except that this figure is shown for the fainter lens system with 2 QSO images in the lens plane.

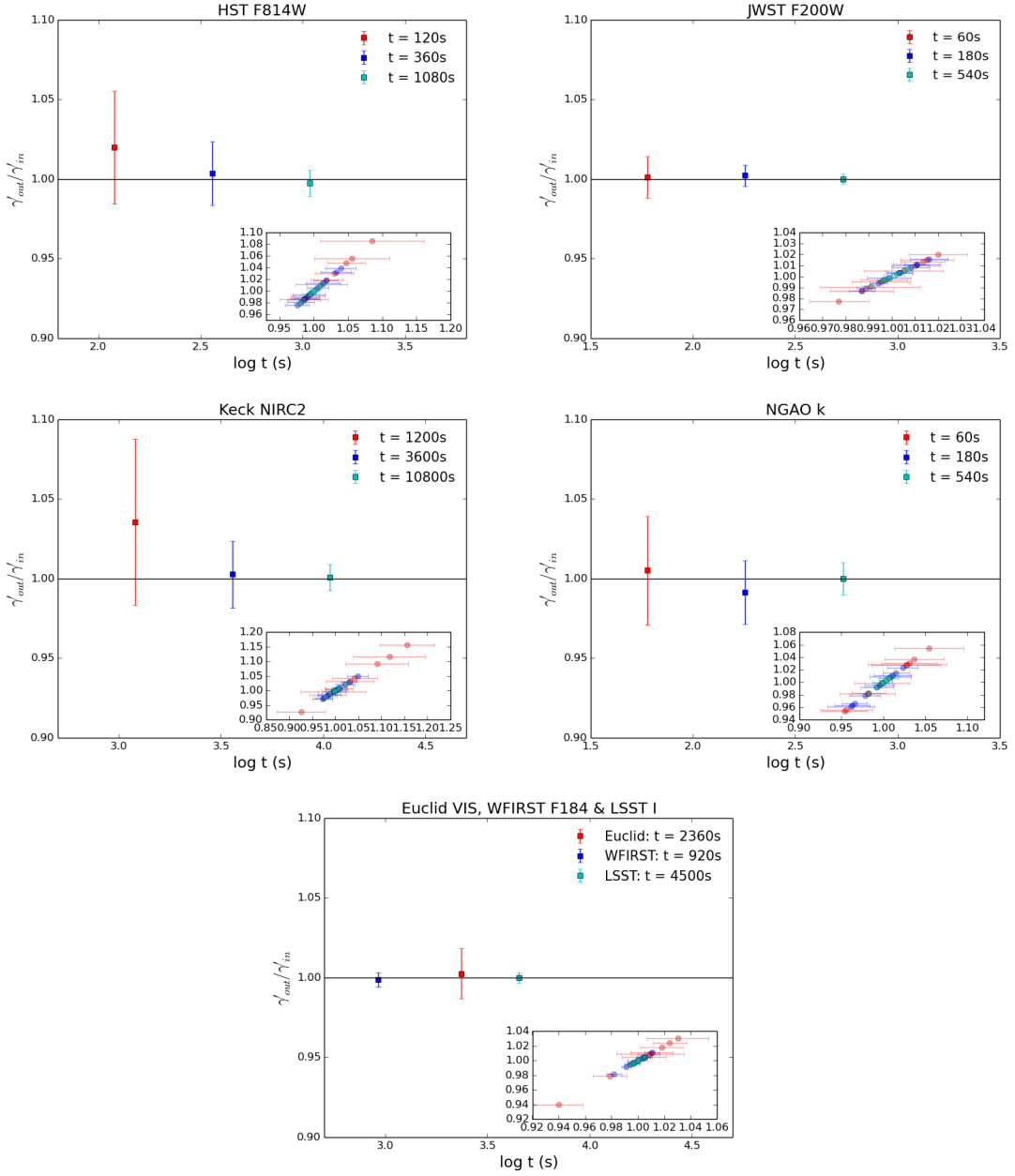


Figure 8. Same as Fig. 6, except that this figure is shown for the brighter lens system with 2 QSO images in the lens plane.

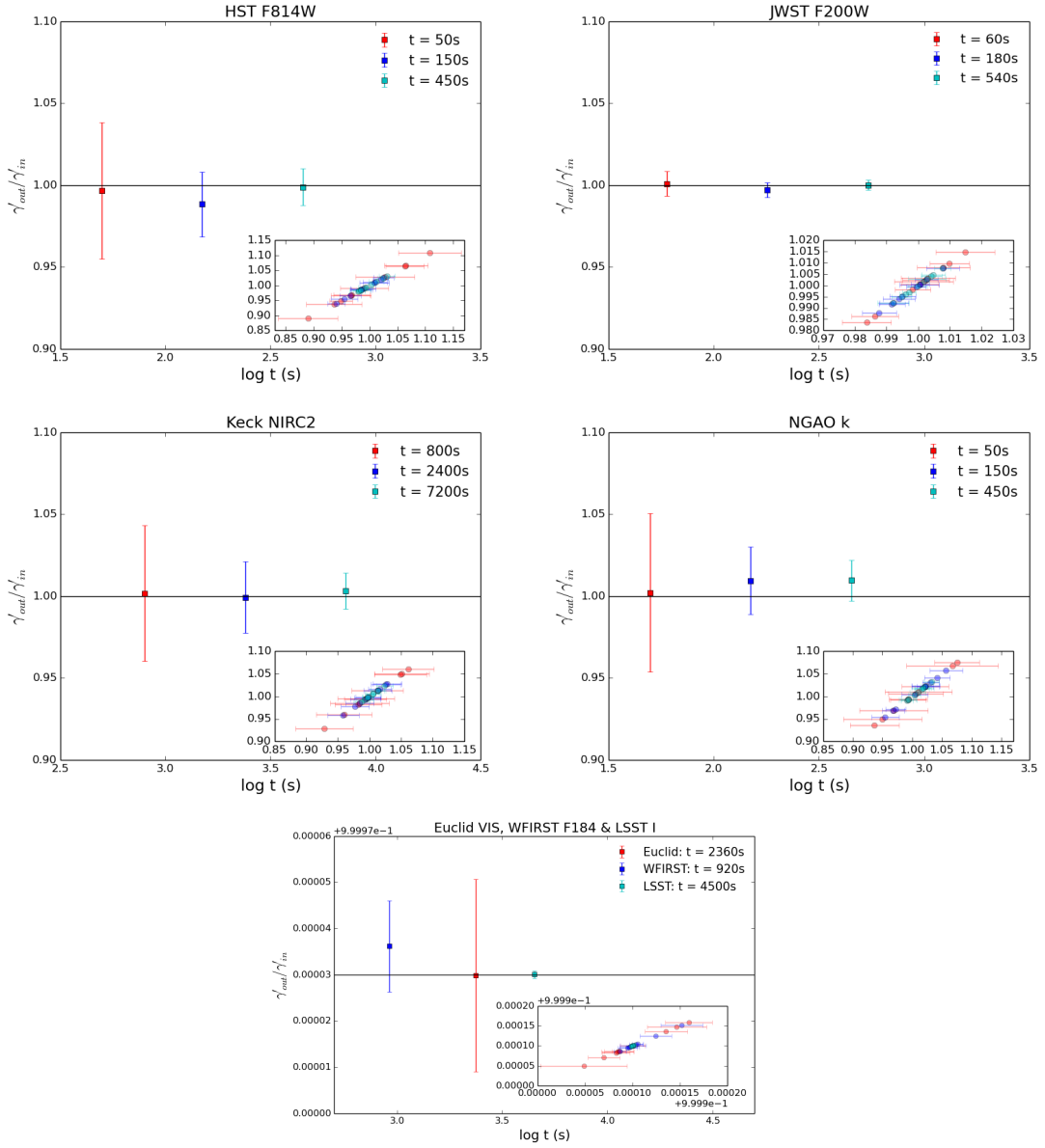


Figure 9. Same as Fig. 6, except that this figure is shown for the brighter lens system with 4 QSO images in the lens plane.